Earth and Planetary Science Letters 559 (2021) 116772

Contents lists available at ScienceDirect

Earth and Planetary Science Letters

www.elsevier.com/locate/epsl

Destructive episodes and morphological rejuvenation during the lifecycles of tectonically active seamounts: Insights from the Gorringe Bank in the NE Atlantic

Davide Gamboa [a,*], Rachid Omira [a,b], Aldina Piedade [a], Pedro Terrinha [a,b], Cristina Roque [b,c], Nevio Zitellini [d]

[a] Instituto Português do Mar e de Atmosfera – IPMA, I.P.; Rua C do Aeroporto, 1749-077 Lisbon, Portugal
[b] Instituto D. Luiz – IDL; Faculdade de Ciências da Universidade de Lisboa, Campo Grande, Edifício C8, Piso 3, 1749-016 Lisbon, Portugal
[c] Estrutura de Missão de Extensão da Plataforma Continental – EMEPC; Rua Costa Pinto, n. 165, 2770-047 Paço de Arcos, Portugal
[d] Istituto di Scienze Marine (ISMAR), Via Gobetti 101, 40129, Bologna, Italy

ARTICLE INFO

Article history:
Received 25 July 2020
Received in revised form 2 December 2020
Accepted 19 January 2021
Available online xxxx
Editor: J.P. Avouac

Keywords:
tectonic seamounts
Mass-Transport Deposits
seamount lifecycle
morphological rejuvenation
evolutionary model

ABSTRACT

Seamounts are spectacular bathymetric features common within volcanic and tectonically active continental margins. During their lifecycles, they evolve through stages of construction and destruction. The latter are marked by variable magnitude flank collapses that often interrupt the evolution of seamounts and constitute a major source of hazard. The Southwest Iberian Margin is a tectonically complex region with moderate to high seismicity where numerous seamounts occur. On such a setting, earthquake-triggered collapses on seamount flanks are common, leading to the deposition of Mass-Transport Deposits (MTDs) on the surrounding abyssal plains. Using a wealth of 2D seismic reflection profiles, we investigate the lifecycle of the tectonic Gorringe Bank (GB), the largest submarine seamount offshore European margins, based on the magnitude and recurrence patterns of MTDs along the active thrust flank. Eight MTDs with relevant expression on the seismic data were analysed, four of estimated Miocene age and four on a Pliocene-Quaternary interval. Miocene MTDs are overall larger and correlate with the main uplift stages of the GB structure. Their distribution and relative timing suggest that failure-triggering earthquakes were common along the whole length of the GB. Pliocene to Quaternary MTDs tend to cluster along the northern half of the GB flank and are generally smaller. Overall, the size and magnitude of the mass-waste events is directly relatable to the magnitude of the uplift stages. Given the lack of indicators of large MTDs on the modern GB morphology, we propose that the lifecycle of tectonic seamounts is marked by morphological rejuvenation driven by thrust fault activity in between major collapse events or cycles. Tectonic-driven rejuvenation is thus key to hinder or obliterate evidence of past high-magnitude destructive events on tectonic seamount morphology.

1. Introduction

Seamounts are spectacular bathymetric features that represent about 21% of the globe seafloor (Hunt and Jarvis, 2020), yet despite their abundance, they are seldom studied in detail (less than 1%) (Staudigel and Clague, 2010). Beyond their importance as seafloor geomorphic features that require detailed mapping and identification (Staudigel and Clague, 2010), seamounts reaching shallower oceanic domains create upwelling sites and isolated biodiversity hotspots hosting a variety of marine life of special conservation interest (Hunt and Jarvis, 2020 and references therein). Moreover, seamounts are of increasing importance as economic resources for deep-sea mining due to the variety of minerals deposits on, or within them (Sarma et al., 1998). The morphology and evolution of these impressive submarine features are controlled by their inception processes and locations. The majority of seamounts is associated with submarine intraplate igneous activity, thus growing near volcanic vents at spreading ridges, hotspots, or above convergent plate boundaries (Schmidt and Schmincke, 2000). Non-volcanic seamounts created by tectonic processes are comparatively less common, but no less important to understand the evolution of oceanic domains. Their uplift stages are associated with transform and/or thrust fault activity in transpressive, transtensional or purely compressional tectonic regimes, typically originating ridge-

* Corresponding author.
E-mail address: davide.gamboa@ipma.pt (D. Gamboa).

https://doi.org/10.1016/j.epsl.2021.116772
0012-821X/

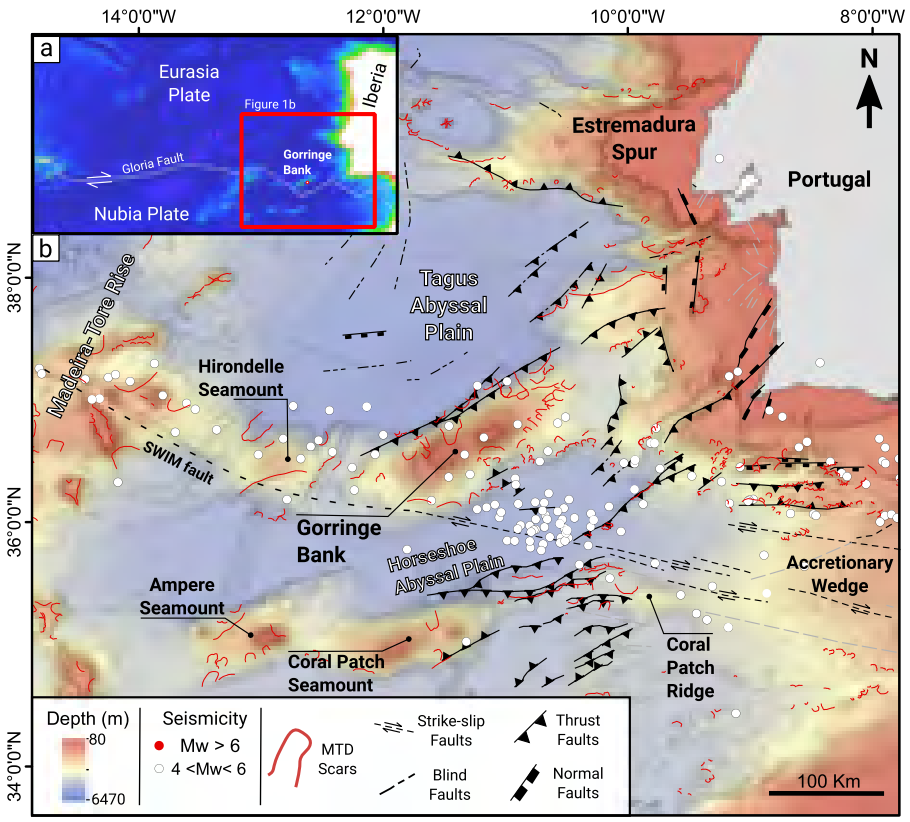

Fig. 1. Regional map of the Southwest Iberian Margin highlighting the major morphological and tectonic features. (For interpretation of the references to colour in this figure, the reader is referred to the web version of this article.)

shaped seamounts and islands (Palmiotto et al., 2017; Schmidt and Schmincke, 2000).

Isles and seamounts worldwide experience continuous constructive and destructive episodes during their lifecycles, inferred from their heterogeneous lithological composition and geomorphology (Hunt and Jarvis, 2020). Large collapses on the seamount flanks characterise the destructive episodes and express as marked geomorphological scars and wide mass-waste deposits on the surrounding seafloor (Mitchell, 2003). Given the variable properties and geometries of the remobilized strata, the term Mass-Transport Deposit (MTD) has been adopted to refer to such features on the subaqueous domain (Posamentier and Martinsen, 2011). MTDs can occur at various dimensional scales and present heterogeneous internal deformation (Moscardelli and Wood, 2016; Posamentier and Martinsen, 2011). Large coherent blocks are often present (Bull et al., 2009), being particularly common on MTDs derived from islands and seamounts (Siebert, 1984). It is common to identify sequences of stacked MTDs in tectonically active areas with recurrent slope failure events (Moscardelli and Wood, 2016). Understanding the recurrence patterns of seamount MTDs is an open challenge, derived from the limited data available to address the question. While recent failure events can be estimated from bathymetric and shallow sub-seafloor sampling, little is known of the magnitude and character of MTDs associated with the broader seamount lifecycle (Hunt and Jarvis, 2020). However, past events are crucial to understand the evolution of seamounts and, thus, to assess future collapse events on their flanks. Such an assessment helps mitigating seamount MTD-induced geohazards as they can compromise the safety of seafloor and subsurface infrastructures (Masson et al., 2006). A growing concern is the tsunamigenic potential of seamount flank collapses due to the high, steep slopes rising hundreds or thousands of metres from the seafloor, and lithological compositions that favour fast evacuating flows (Lo Iacono et al., 2012; Omira et al., 2016; Tontini et al., 2013).

Seamounts are prevalent on the Madeira-Tore Rise and proximal domains of the Southwest Iberian Margin (SWIM) (Fig. 1). The SWIM is a tectonically complex region with significant seismicity related to the interaction between the Southern Eurasia and Africa (Nubia) tectonic plates (Purdy, 1975; Zitellini et al., 2009). Large earthquakes have originated on the margin as the 1755 Lisbon Earthquake (Mw $\sim$ 8.5) and associated tsunami, the 1969 earthquake (Mw = 7.9) or the 2007 Horseshoe earthquake (Mw = 6.0) are examples of important events (Baptista et al., 1996; Fukao, 1973; Zitellini et al., 2001). As submarine earthquakes are widely recognised as triggers for slope instability (Posamentier and Martinsen, 2011), mass-wasting on the flanks of the SWIM seamounts pose a serious geohazard to the surrounding European and northern African coastal areas (Omira et al., 2016). Numerous seamounts are present on the SWIM, which include the Gorringe Bank (GB), the largest seamount on European offshore domains (Fig. 1). It rises from the abyssal plain depths of 5000 m to the top at 30 m as a result of major thrust tectonics that uplifted mantle-related lithologies (Sartori et al., 1994; Girardeau et al., 1998; Sallarès et al., 2013). Mass-failure scars are observed on the present-day morphology of the northern flank of the GB (Fig. 1), of which a prominent one is associated with a blocky MTD (Lo Iacono et al., 2012). However, limited proof of past large-scale mass-failures can be observed on seafloor data of the Tagus Abyssal Plain (TAP), despite the identification of sizable MTDs along the northern flank of the GB as a result of its exhumation and continuous uplift (Jiménez-Munt et al., 2010).

If the lack of known long-term geological records is a major knowledge gap to understand the magnitude, recurrence and triggers of mass-failures on volcanic seamounts (Hunt and Jarvis, 2020), this is probably of higher relevance to understand the tec-

tonic processes. We here use the Gorringe Bank as a prime example to understand the recurrence patterns and 3D distribution of MTDs along a tectonic seamount's active front, and how these relate to major tectonic stages of its lifecycle. Through this study we aim to investigate if: 1) strata adjacent to the tectonically active flanks of tectonic seamounts record constructive and destructive cycles when compared to volcanic seamounts dominated by destructive cycles; 2) tectonic seamounts are prone to ongoing morphological rejuvenation, attenuating evidence of past collapses; and 3) MTDs can provide clues of the timing and locus of activity on tectonic seamounts. We also aim to bring insights on the role of MTDs to assess the evolution of, and geohazards associated to tectonic seamounts present on active margins or ocean domains.

2. Geological and seismotectonic setting

The continental margins of Iberia are surrounded by rifted margins to which oceanic lithosphere has been welded as the result of various tectonic processes such as, the formation of the North-East Atlantic (Early Cretaceous), the ∼35° rotation of Iberia (Late Cretaceous-Early Cenozoic), the formation of the Neo-Tethyan ocean floor in Jurassic times, and the formation of back-arc basins in the West Mediterranean realm associated to the South Iberia Tethyan Ocean subduction in Oligocene through Present times (Vergés et al., 2019 and references therein). These include Miocene tectonic compressive events associated with the Alpine orogeny, which led to the reactivation and inversion of major rift faults on the Iberian Margin (Ramos et al., 2017). The Southwest Iberian Margin (SWIM) extends between the latitudes of the Estremadura Spur pop-up (Neves et al., 2009) and the Gibraltar Strait, and to the west is limited by the Madeira Tore Rise (MTR) overthickened oceanic crust (Peirce and Barton, 1991). The SWIM boundary to the Africa plate (Nubia sub-plate) is marked by two lithospheric-scale structures, the Gibraltar subduction (Gutscher et al., 2002) and the SWIM Fault transform plate boundary (Zitellini et al., 2009). However, the Gibraltar Accretionary Wedge overthrust by the Gibraltar Arc has dramatically diminished its rate of activity from Pliocene through Present or even ceased (Zitellini et al., 2009).

The SWIM Fault intersects the MTR as it links with the Gloria Fault (Fig. 1). These faults constitute the Africa-Eurasia transform plate boundary from the western tip of the Azores plateau to Gibraltar. The current Nubia-Iberia ∼ NW-SE convergence is slow (3.8–5.6 mm/yr.), with Pliocene-Quaternary deformation being accommodated to the north of the SWIM Fault by NE-SW and E-W striking thrusts (Grevemeyer et al., 2017). To the north of the plate boundary, the MTR is made up of Cretaceous seamounts while to the south these are predominantly Neogene-Quaternary (Geldmacher et al., 2006). Regional seismicity concentrates to the north of the SWIM Fault in the Horseshoe Abyssal Plain and along the Josephine-Gorringe Ridge (Fig. 1b), coincident with the occurrence of the largest landslides in the Quaternary (Omira et al., 2016).

The SWIM and adjacent domains are interpreted as a diffuse tectonic boundary with moderate seismicity concentrated along a ∼1500 km long, 200 km wide belt that underlies Iberia's Southwest and Southeast contacts with Northeast Africa (Zitellini et al., 2009). Most of seismicity is of small-to-moderate magnitude, generated in the lithospheric mantle between 30 km and 80 km by means of thrusting and strike-slip events related to the collision of the European and African plates, compatible with a NW-SE Sh_{max} (Custódio et al., 2015). Seismic events recorded between 1961 and 2020 (n = 11879, 1806 pre-January 2000) indicate Mw = 3 or lower account for circa 90% of occurrences, with only sixteen events Mw > 5. However, the latter include large and destructive earthquakes and tsunamis, such as the 1755 Lisbon (Mw ∼8.5–8.7) and the 1969 Horseshoe (Mw = 7.9) events (Baptista et al., 1996; Fukao, 1973). Ocean Bottom Seismometers records in the Horseshoe Abyssal Plain show seismicity clusters localized at the intersection of the SWIM Fault with NE-SW striking thrusts, the Horseshoe, S. Vincent and Gorringe clusters (Silva et al., 2017). Focal mechanisms indicate that towards the SW and NE limits of the GB cluster strike-slip motions prevail, while on the central area reverse and oblique slip motions occur, parallel to the Gorringe Thrust Fault (Silva et al., 2017; Zitellini et al., 2009).

The Gorringe Bank is a 5 km high, 200 km long, and 80 km wide piece of lithospheric mantle overthrust on top of the Tagus Abyssal Plain (Fig. 2). Earthquake focal mechanisms show a progressive shift from the strike-slip motion to compression within a domain comprising the GB and part of the Horseshoe Abyssal Plain where NNW-trending thrust faults were identified (Tortella et al., 1997; Zitellini et al., 2009). The age of thrusting and main GB uplift is supposed to be Mid-Miocene and the total amount of transport is 15 to 20 km (Sartori et al., 1994; Jiménez-Munt et al., 2010). The main uplift and thrusting events are probably the same as occurred at the seamounts to the south and north (Fig. 1) (Neves et al., 2009). However, seismicity is at present mostly localized along the Josephine-Gorringe seamounts. The GB basement rocks correspond to serpentinised peridotites, cataclastic gabbros and mylonites, tholeiitic basalts and alkaline rocks (Girardeau et al., 1998) emplaced in distinct tectonomagmatic episodes during the Early Cretaceous and beginning of the Paleogene (Sallarès et al., 2013). These lithologies are overlain by a thin cover of sediments (Girardeau et al., 1998). The Ormonde and Gettysburgh seamounts (Fig. 2) are mainly constituted by lithospheric mantle rocks and crustal rocks intruded by the Early Cenozoic alkaline magmatic bodies. The saddle between these two peaks probably corresponds to an extensional lithospheric detachment (Rovere et al., 2004) to which mylonitic extensional fabrics were reported (Girardeau et al., 1998).

The seismic-stratigraphic framework for the TAP has been established following Mauffret et al. (1989), Sartori et al. (1994), Tortella et al. (1997) and Neves et al. (2009). Sartori et al. (1994) identified a Mid-Miocene Unconformity, equivalent to the Lower Miocene boundary of Neves et al. (2009) (Fig. 3 and Supplementary Material 1). This is a regional marker delimiting the top of tectonised Mesozoic to Lower Miocene strata. Reflectors on the overlying Upper Miocene to Holocene strata are sub-horizontal and show less intense deformation (Neves et al., 2009). The Mesozoic to Lower Miocene sequences overlying the basement are likely composed of Aptian marls and limestones, Upper Cretaceous shales with limestone and cherts, and Lower Cenozoic silty mud and pelagic sediments (Tortella et al., 1997) (Fig. 3). The Miocene to Quaternary strata generally comprises alternating sequences of turbidites and pelagic oozes (Gràcia et al., 2010; Tortella et al., 1997).

3. Data and methodology

The bathymetric data used is the 2018 version of the EMODnet DTM for European seas covering the Southeast Iberian margin (EMODnet Bathymetry Consortium, 2018), integrating the high-resolution SWIM grid from Zitellini et al. (2009) (Fig. 2). The general grid resolution is circa 115 m. Bathymetric profiles of the seafloor morphology were obtained along the path of seismic profiles in order to quantify slope gradients along the GB (Supplementary Material 2). The 2D multi-channel seismic reflection data used in this study intersect the GB and variably extend into the adjacent TAP. These were acquired during multiple oceanographic expeditions and include profiles from the BIGSETS (Gràcia et al., 2003; Zitellini et al., 2001), IAM (Banda et al., 1995) and ARRIFANO campaigns (Sartori et al., 1994), complemented by data acquired by TGS. Details of the seismic data parameters are listed on Supplementary Material 3.

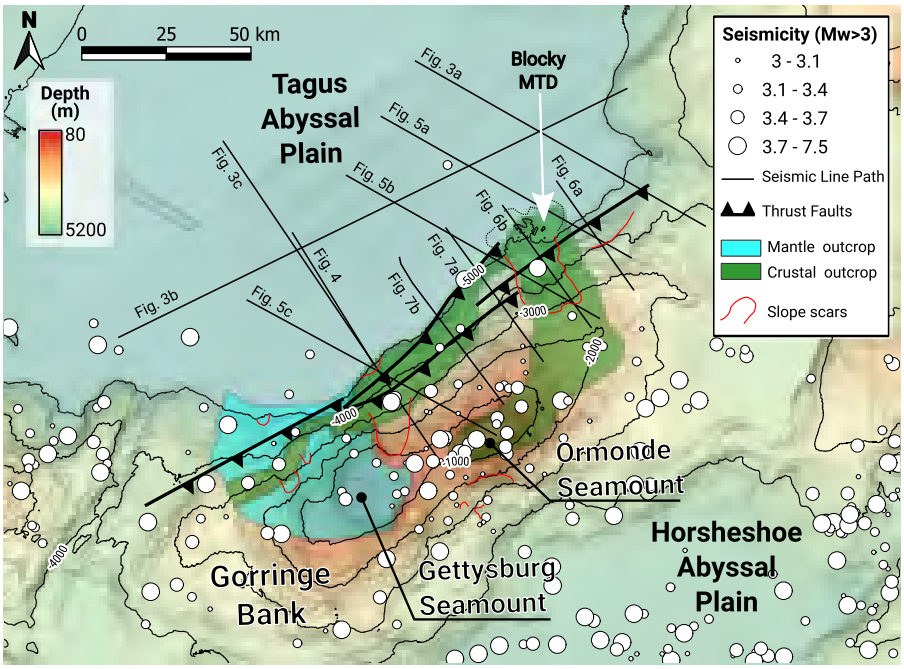

Fig. 2. Morphological map of the Gorringe Bank and surrounding Tagus and Horseshoe Abyssal Plains. Four main thrust fault segments compose the frontal thrust domain. White circles represent earthquake epicentres with Mw > 3, with several occurrences on the Gorringe Bank and Horseshoe Abyssal Plain. Several slide scars occur on northern flank of the Gorringe Bank, but there is limited expression of MTDs on the modern Tagus Abyssal Plain seafloor. The seismic line paths (black straight lines) indicate the 2D seismic coverage used in this work. Bathymetric data from EMODnet Bathymetry Consortium (2018) and Zitellini et al. (2009).

The mapping of MTDs on the seismic profiles (Fig. 3 and Supplementary Material 4) was based on the identification of seismic facies with a chaotic or mottled character, with generally low to moderate amplitude and broken reflections (Posamentier and Martinsen, 2011). Top and base surfaces of each individualised MTD were mapped. The top horizon commonly expresses an irregular topography, while the base horizon is generally flatter with occasional steps or ramps. Internal deformation of the submarine landslide strata was analysed following the identification of folded reflections, extensional faults and imbricated internal thrusts, all of which constitute mass-flow kinematic markers (Bull et al., 2009). The separation of individualised MTDs, where stacked deposits occur, rests on the identification of their basal shear intervals, and internal folds and faults vertically bounded by them (Bull et al., 2009). High-amplitude features can occur (Fig. 4) particularly when rafted blocks are present, which consist of coherent portions of remobilised strata resting, or entrenched, at the basal shear intervals (Bull et al., 2009). Seismic attributes were used to improve the visualisation of the 2D vertical profiles. A structural filter with fault preservation was used. The attribute applies a coherency filter to the data, improving reflection continuity along dominant dips while preserving faults and discontinuities (Chopra and Marfurt, 2007). This improves data visualisation and expresses the broken-up nature of reflections of the original data as clearer continuous events. A pseudo-relief attribute derived from a phase rotation on RMS amplitude seismic attributes (Bulhões and de Amorim, 2005) was applied to the data to produce seismic textures emphasizing strata contrasts and deformation features.

4. Results

4.1. Morphology of the Gorringe Bank northern flank

Six bathymetric profiles were obtained along the northern flank of the GB (Supplementary Material 2), five along the 2D seismic profiles (Fig. 2) and an additional one where no seismic profiles are available. Across-flank gradient patterns change between the Ormonde-Gettysburg saddle and the northern limit of the GB (profiles BS13 to IAM4, Supplementary Material 2). Gradients on the latter area range between 5° to 7° at the upper flank towards the summit. At mid-flank positions, between 3000 m and 4000 m depth, steeper gradients are observed between 8° to 10°. Towards the base of the flank, gradients decrease to 5°–7°, influenced by strata deformation processes at the thrust front and gravitational flows. The main exception to the gradient trends is observed along profile BS14, which intersects an MTD. The steeper gradients up to 11° are recorded within the scar evacuation domain, decreasing downslope to 1.4° along the depositional area. Steeper values near 9° are observed at the base of profile IAM-4 where a scar is present near the base. Contrasting with the northern GB slope trends are the much steeper gradients along the southwest-most profile. Here, gradients reach 15° on the upper half of the flank, decreasing to 12° towards the base (Fig. 5). However, the decrease at the base may be influenced by tectonic and/or gravitational processes, although the latter seem less obvious in this area.

4.2. Character and distribution of Mass-Transport Deposits

Several MTDs that originated on the northern flank of the GB and flowed towards the TAP were interpreted on the 2D seismic data. As we focus on features on the northern flank of the GB, future references to northern and southern sectors will relate to the respective half along the GB length. Eight MTDs with relevant acoustic signatures were identified, seven being fully buried and one has expression on the seafloor (Figs. 3 to 7). The low seismic data coverage limits the full spatial analysis of the MTDs (Fig. 2), yet a viable assessment is possible where profiles intersect. The mapped MTDs occur above the reference horizon H1, estimated as the base of Upper Miocene, except for MTD1 estimated to be of (Lower?)/Middle Miocene age (Figs. 3 and 4).

The MTD nomenclature follows a relative timing assessment, possible where their lateral and vertical offsets are identifiable (Fig. 3b). Morphometric parameters of the MTDs were obtained and are summarised in Supplementary Material 4 and 5.

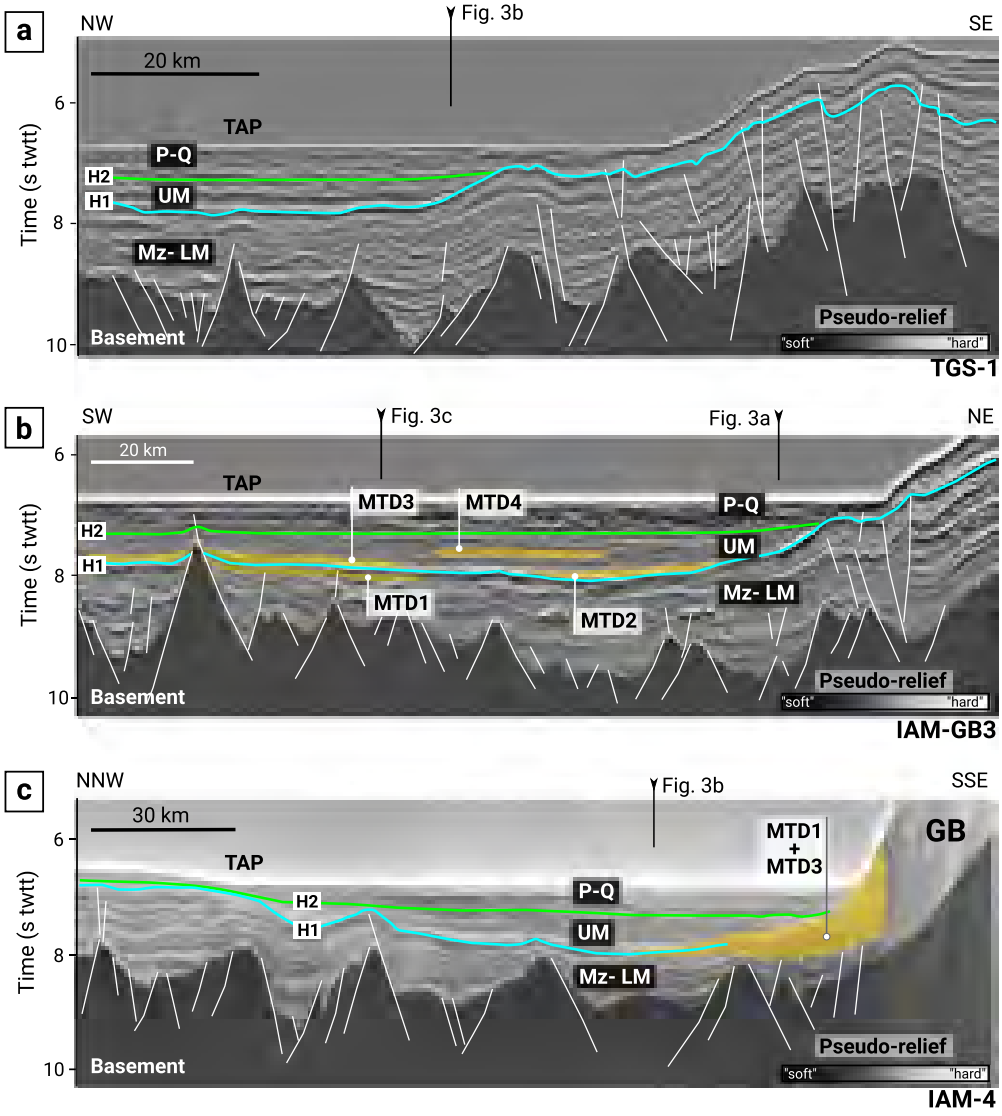

Fig. 3. Representative seismic profiles of the Tagus Abyssal Plain (TAP) and Gorringe Bank's (GB) flank, displayed using the pseudo-relief attribute. The basement is characterised by fault-bound grabens and half-grabens, overlain by a sedimentary cover that can reach a maximum of 5 km (Neves et al., 2009). Three main seismo-stratigraphic units were defined for the purpose of this study, namely: Mz-LM, with undifferentiated Mesozoic to Lower Miocene strata; UM with Upper Miocene Strata; P-Q with Lower Pliocene to Quaternary Strata. Two reference horizons, H1 and H2, delimit these seismic packages. Large MTDs are outlined in yellow.

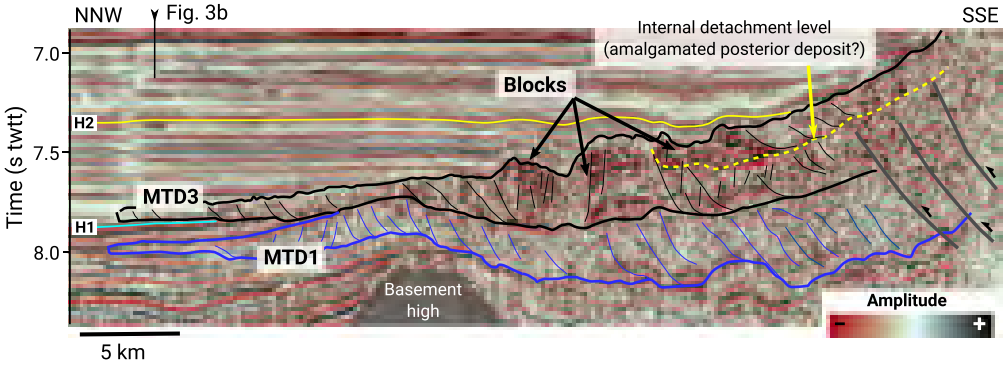

Fig. 4. Seismic profile AR-3 showing two of the older MTDs. While the majority of the deposits are amalgamated, the gap between their frontal toe suggests a relevant time interval between their occurrence. Imbricate, SSE-dipping internal thrusts predominate in the deposits as a result of the depositional process but posterior deformation is likely to have occurred due to regional thrusting. Slide blocks are present on MTD3, suggesting emplacement by a flow with large coherent lithologies derived from the Gorringe Bank. Towards the SSE the limit of the MTDs is not clear, likely due to posterior deformation and inclusion on a tectonic mélange at the thrust front.

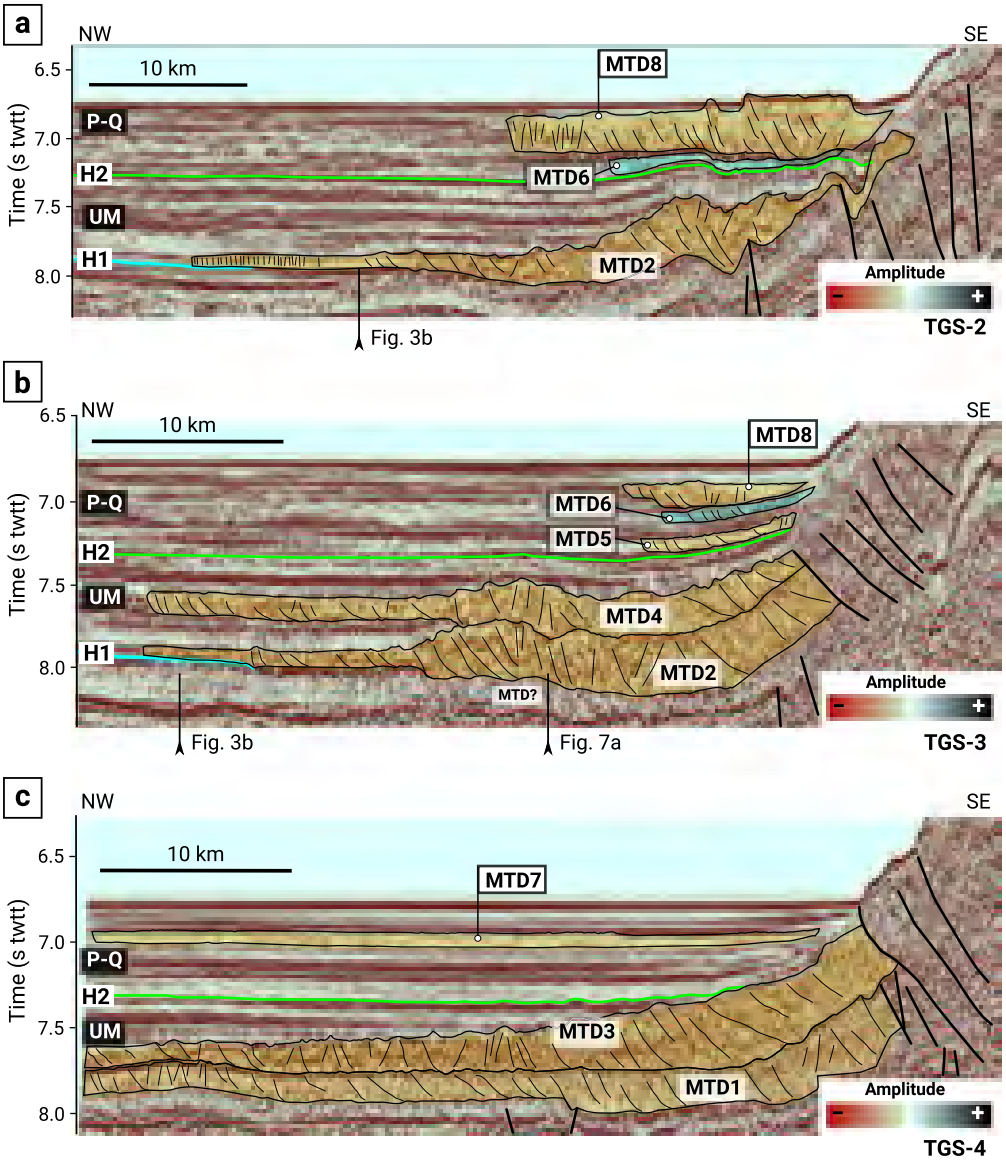

Fig. 5. TGS seismic profiles depicting MTDs in the studied intervals. The majority of deposits are characterised by numerous internal thrusts, concordant with emplacement from the flanks of bathymetric highs but post-depositional deformation may have occurred. Upper Miocene (UM) MTDs are generally longer and thicker when compared to Plio-Quaternary (P-Q) ones. Post-depositional deformation of MTD2 and MTD6 by folding and fault offset is clearly visible in **a)**, but less clear or absent in **b)** and **c)**. Such indicates younger deformation events located towards the north.

The oldest deposit is MTD1, located towards the southern sector of the GB (Fig. 4). It occurs immediately below horizon H1, thus placing it within the top strata of the Lower/Middle Miocene. Yet, its inclusion in this analysis is relevant as it is overlain by the similarly large MTD3 (Figs. 4 and 5). The internal character on the proximal domain exhibits imbricated reflections resultant from internal compression which are truncated by the top surface. Primary ones are syn-depositional, yet there may be secondary compressional features created, or enhanced, by loading of the overlying deposit and posterior tectonic activity. These processes likely altered the top morphology of MTD1 and its original thickness. It is possible that other MTDs of Middle Miocene age have occurred on other areas flanking the GB. An example of this can be the seismic package partially underlying MTD2 (Fig. 5b).

Resting on horizon H1, MTD2 was emplaced along most of the northern sector of the GB (Figs. 3b, 5, 6, 7 and 8b). Variable internal amplitudes are observed in it, aiding the identification of internal imbrications. Internal sub-horizontal interfaces extending along significant portions of MTD2 are discernible (Figs. 5b and 6b). These represent internal detachment surfaces, either syn-depositional or influenced by posterior deformation. The width towards the toe is lower than the width adjacent to the GB flank (Fig. 8b), possibly due to a structural control of the accommodation space towards the distal TAP, as demonstrated by the lateral pinch-out of the MTD (Fig. 3b). The MTD thickness patterns are variable, partially influenced by the overlying MTD4 (Figs. 5b, 6b and 7), but generally decrease towards the toe. MTD2 is deformed near its northern limit where several faults are observed (Fig. 5a), in addition to the general proximal titling of the older MTDs imposed by the advancing thrust front. However, the same is not observed southwestwards (Fig. 6a).

MTD3 was deposited towards the limit of the GB southern sector, overlying MTD1 (Fig. 3b). The undeformed strata intercalated between their toe region indicate a time gap between collapse events (Figs. 3b and 4), but it is not possible to quantify it. MTD3 shows gradual thinning, culminating at a small frontal ramp (Fig. 4). However, its deposition was controlled by paleotopographic seafloor irregularities derived from basement struc-

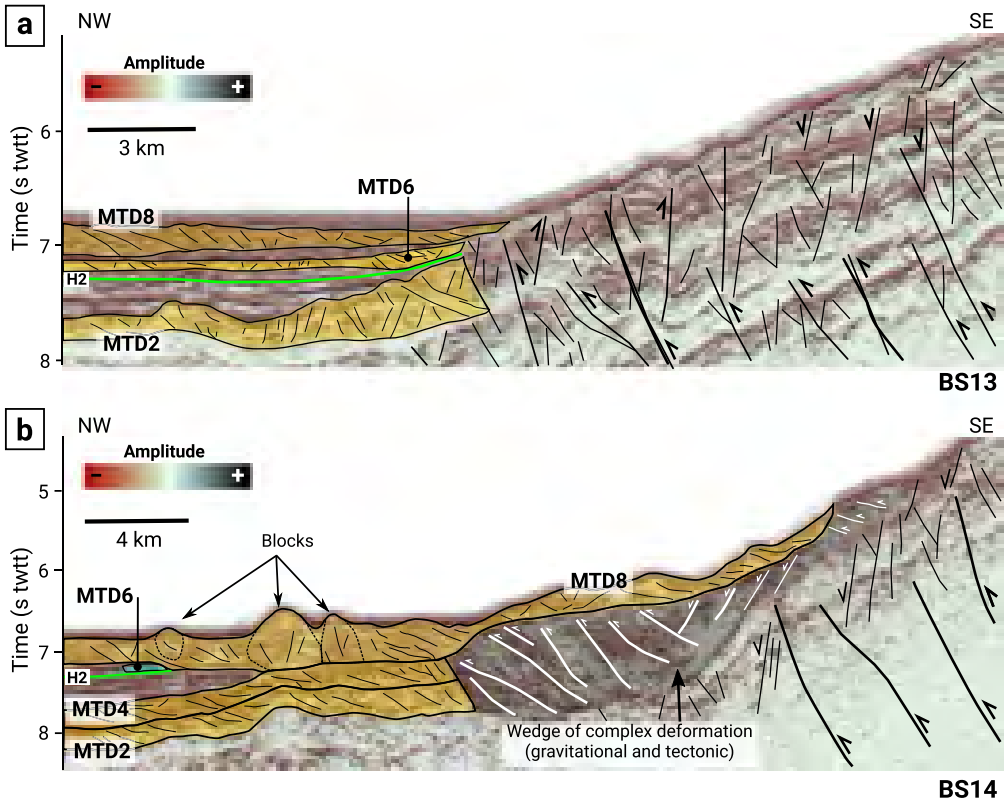

Fig. 6. BIGSETS seismic profiles displayed as pseudo-relief with an amplitude overlay. **a)** Three MTDs are observed. The section of MTD8 here present is fully buried and with no seafloor expression. Towards the SE thrust and reverse faults occur with limited gravitational deformation. **b)** Profile depicting the main section of MTD8, evidencing large blocks and seafloor expression. Here, MTD8 partially obliterated the pre-existing MTD6 and MTD4. A wedge of predominant compressional deformation features of gravitational and tectonic origin is observed, and has been partially remobilised by the younger mass-failure.

tures, which inclusively forced a slight split at the MTD front (Fig. 3b). Internal thrust imbrications occur along the length of MTD3, and high-amplitude blocks within the deposit also mark morphological pinnacles on its top surface (Figs. 4 and 5c). Intra-MTD sub-horizontal amplitude interfaces suggest either a complex emplacement with internal detachments, or an eventual amalgamated posterior deposit. The latter is plausible, but not possible to confirm with the current data coverage.

MTD4 is the youngest of the deposits interpreted within the Upper Miocene interval (Figs. 5b and 7b). It is adjacent to the central/northern sector of the GB (Fig. 8d). The MTD top surface is irregular and punctuated by mounded geometries often coincident with thicker accumulations, but no discernible slide blocks are observed on the seismic data (Figs. 5b, 6b, 7b). The MTD is frontally confined by a ramp delimiting a toe with numerous imbricated thrusts (Fig. 5b). While most of the deposit is buried under horizon H2, the latter onlaps the top of MTD4 at points (Fig. 7b). This is more evident towards the centre of the GB, suggesting that MTD4 created significant relief on the paleo-morphology of the basin. Internal amplitude variations highlight thrust imbrications and folding. An internal interface is also identifiable, particularly where it delimits contrasting amplitude packages (Fig. 7).

Within the Pliocene-Quaternary strata package delimited by horizon H2 and the seafloor, MTD5 is the oldest and the smallest of the deposits (Figs. 5 and 8e). MTD5 partially erodes H2 on the proximal area, with the mid and frontal sections overlying it (Fig. 7a). It is markedly thinner than the older deposits below H2. The true lateral extent of MTD5 may be wider than what was assessed, or equivalent deposits may have occurred at the same stratigraphic level, but this cannot be confirmed.

The next deposit on the sequence is MTD6, which may have been emplaced a relatively short time after MTD5. Contrasting with the other deposits, MTD6 has a short length and comparatively larger width (Supplementary Material 4 and 5, Fig. 8f). While near the centre of the GB the base of MTD6 is about 150 to 200 ms twtt above H2, towards the northern sector MTD6 rests on H2 where this horizon onlaps the flank of the paleo-TAP basin (Figs. 3a, 3b). There is the possibility that MTD6 is composed of two (or more) deposits located at the same stratigraphic level, as observed elsewhere for seafloor MTDs derived from the flank of elongated tectonic ridges (Gamboa and Alves, 2016). The thicker accumulations towards the edges of MTD6 can support this alternative (Fig. 8f). Internal thrusts are common in MTD6, frequently extending towards or near the top surface, and intra-MTD reflection preservation is variable within its extent (Figs. 5 and 6a). At places, the deposit is deformed and cannibalised by the bulk of the overlying MTD8 (Fig. 6b).

Contrasting with the location of most Pliocene-Quaternary MTDs, MTD7 occurs on the southern sector of the GB (Fig. 8g). It is one of the thinner and shallowest of the MTDs analysed, buried under a package 150-220 ms twtt thick below the seafloor (Fig. 5c). It is thicker to the west, thinning towards the north and east. However, the thickness estimation to the latter sector may be inaccurate due to limited data for surface interpolation. The internal facies are generally uniform within the MTD extent, characterised by mottled and disrupted reflections but semi-continuous irregular ones are also observed (Fig. 5c). MTD7 occurs at the general stratigraphic level of the much larger MTD8, possibly indicating a common regional event, or short spaced ones, for the genesis of both.

The clearest collapse feature on the GB is MTD8, otherwise known as the North Gorringe Avalanche (Sallarès et al., 2013; Lo Iacono et al., 2012). It shows a clear scarp on the modern GB morphology and several block pinnacles within a lobate relief on

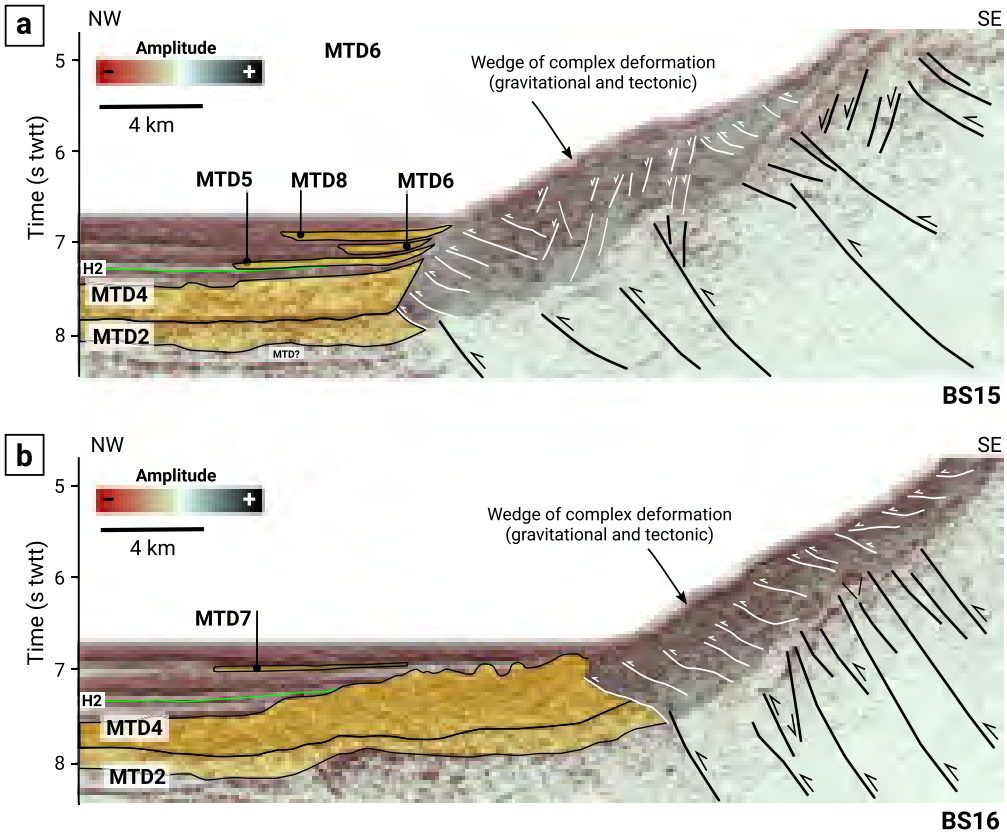

Fig. 7. BIGSETS seismic profiles displayed as pseudo-relief with an amplitude overlay. **a)** Section showing the clear size contrast between Upper Miocene and Plio-Quaternary MTDs. The deformation wedge features are well observed, with compressional structures at the front and back but extension occurs at central areas. **b)** Section intersecting the central domains of the Gorringe Bank where the large Miocene MTDs occur, but later ones are scarce and only represented by the thin MTD7. Numerous thrust deformation features are observed on the flank and may induce future failures on the area.

the seafloor (Figs. 2, 6b and Supplementary Material 1). The sediment overlying MTD8 reaches 115 ms twtt (circa 100 m) at its toe limit (Fig. 5a). The wider dataset available for our study also shows that MTD8 is larger than previously described by Lo Iacono et al. (2012). It has a length of 43.7 km from scarp to toe, exceeding the previously described length of 35 km. This can be split as 21.3 km within the headwall domain and 22.4 km within the depositional domain in the TAP. We estimate a depositional area of 684 km^2, over the double of the 300 km^2 from Lo Iacono et al. (2012). The bulk mass of MTD8 is within the central area where it is up to 830 ms twtt thick and large slide blocks are present. While in the central area the base surface of MTD8 intersects older mass-flow deposits (e.g. MTD5, Fig. 6 and MTD4, Fig. 7b), it shallows towards the outer edges (Fig. 5b). The MTD is confined at the toe limit by a ramp, which is stepped at places. Internal blocks are common within the remobilised mass, evidenced by higher amplitudes, and internal thrusts occur widely in the deposit (Fig. 5 and 6b).

Direct morphometric comparisons between MTDs within the Upper Miocene - Plio-Quaternary seismo-stratigraphic units have limitations since their source areas are not known, with the exception of MTD8, thus limiting their original full-length metrics. Exact thickness estimations would also have to account for accurate depth conversions and compaction effects not undertaken here, which would enhance the size disparity between Miocene and Pliocene-Quaternary MTDs. Despite this, the distinct magnitude of events within the two units is still well represented by the morphometry obtained from the time-based dataset (Supplementary Material 4 and 5).

5. Discussion

5.1. Tectonism and mass-wasting on the Gorringe Bank lifecycle

Ridges created along regional thrust systems are prone to oversteepening and flank collapses associated with tectonic instability cycles (Festa et al., 2016). The resultant MTDs are rather diachronous, and original gravity-driven deformation can be overprinted by tectonic deformation. However, the distribution, size and relative timing of MTDs constitute proxies for the location, chronology and magnitude of relevant regional tectonic episodes (Alves and Gamboa, 2019). The MTDs analysed in this work bring new insights on the relative magnitude, broad timing and locus of major destructive events at distinct evolutionary stages of the GB. Constructive phases of a seamount's long-term lifecycle, regardless of their nature, lead to their growth as bathymetric highs (Hunt and Jarvis, 2020; Mitchell, 2003). For the GB, these phases are intrinsically related to its fairly constrained exhumation and uplift history, considered to have peaked on the Upper Miocene (Jiménez-Munt et al., 2010).

Mass-flow events result from a combination of spatially and timely constrained preconditioning factors and triggers (Mountjoy et al., 2020). Preconditioning factors for seamount flank collapses include heterogeneous lithologies, faults and fractures networks, and flank steepening (Mitchell, 2003). In the tectonic GB, pervasive fractures and faults are a main preconditioning factor to failure (Lo Iacono et al., 2012), organised as networks of longitudinal NE-SW faults parallel to the main thrust (e.g. Figs. 5 and 6), and N-S faults sub-perpendicular to them (Fig. 9). The latter were observed on the GB top saddle (Ferranti et al., 2014), and inferred from alignments of earthquake epicentres beneath the structure (Silva et al.,

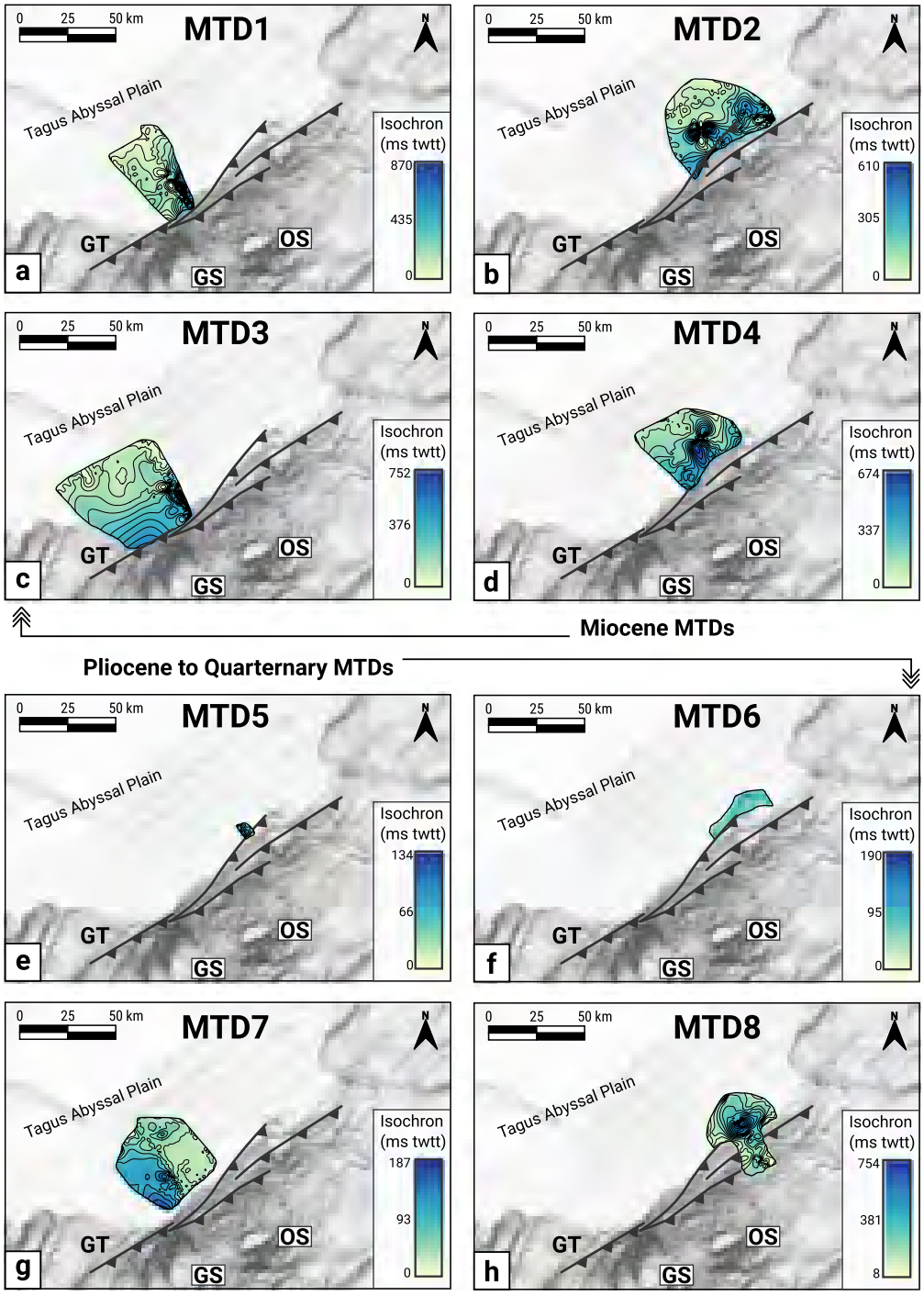

Fig. 8. MTD isochron and extent maps, overlain on the modern seafloor dipmap. **a)** to **d)** show the larger and thicker Miocene MTDs along the whole flank of the GB. **e)** to **h)** show Pliocene to Quaternary MTDs, thinner and of lower extent, predominantly occurring towards the northern and central domains of the Gorringe Bank's flank.

2017). The scar of MTD8, the only clearly related to the interpreted deposits, suggests an influence of fault on MTD limits. It shows sidewalls aligned with N-S faults and a top subparallel to NE-SW-oriented thrusts and faults (Figs. 8h and 9b). Furthermore, its evacuation area is underlain by main thrust faults and by shallower inverse and normal faults (Fig. 6b). Given their shallow reach, the latter may play a role on MTD inception on tectonised morphologies (Fig. 6). A further factor favouring slope failure on the GB is its lithological heterogeneity, consisting of mantellic peridotites with variable degrees of serpentinization, gabbros and basalts, further capped by sedimentary drape units deposited during the seamount's uplift (Girardeau et al., 1998). The lithology distribution supports the structural segmentation in the GB, based on the predominance of outcropping mantellic lithologies to the south, and crustal rocks to the north (Figs. 2 and 9). Therefore, it is likely that the MTDs have a very heterogeneous composition and of distinct ages derived from the crustal or mantellic exposures at their sources, the existing sedimentary cap at the time of collapse, and the abyssal plain sediments entangle within the mass flow. Seismic activity is the likely trigger for flank collapses on the tectonic GB, also considered the main trigger for mass-flows on the broader SWIM (Gràcia et al., 2010). Sea-level changes are another mass-wasting trigger on seamounts (Hunt and Jarvis, 2020). A marked drop on sea-level happened at the transition to the Tortonian (Haq

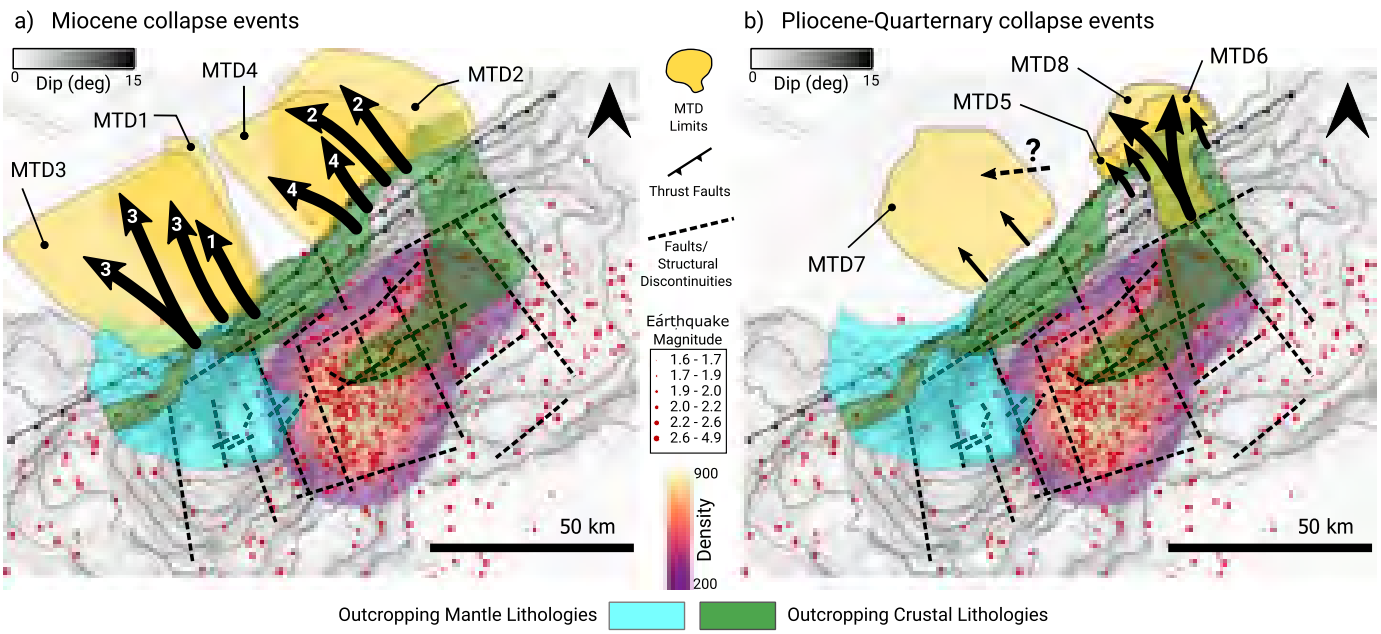

Fig. 9. Diagram of instability on the flanks of the Gorringe Bank and MTD emplacement on the Tagus Abyssal Plain. **a)** Widespread tectonic and instability events occurred along the whole Gorringe Bank during its Miocene main uplift and exhumation stage. This led to the deposition of large, stacked MTDs on the Tagus Abyssal Plain. **b**) Post-Miocene MTDs cluster on the northern sector of the GB, suggesting a predominance of instability events along structures here located, possibly associated with the seismicity cluster. MTD7, the thin but wide deposit mapped in this interval, is the exception and derived from a central Gorringe Bank location. Dashed lines represent the network of faults and structural discontinuities compartmentalising the Gorringe Bank.

et al., 1988), coincident with the relative age of some of the GB MTDs, and Pleistocene sea-level changes shaped the terraces and dismantled sediment atop the GB (Ferranti et al., 2014). However, mass-wasting on the latter still point to a structural control by deep-seated faults rather than an eustatic influence. Thus, although sea-level changes may influence smaller GB collapses, earthquakes and tectonic uplift are the likely main triggers for the major flank collapse events.

The larger MTDs are interpreted as associated with the major GB uplift phase, which started at the Middle Miocene and peaked during the Tortonian (Upper Miocene) (Jiménez-Munt et al., 2010) (Figs. 3, 5 and Supplementary Material 3). The MTDs are amalgamated near the GB flank but vertical offsets between the toe of MTDs with larger length indicate that variable time gaps separated major collapse events (Figs. 3, 4 and 5b). A relevant time gap separates the Lower/Middle Miocene MTD1 (and a possible equivalent underlying MTD2, see Figs. 5 and 7), and the MTDs resting on horizon H1, the base of the Upper Miocene (Figs. 3 and 5). This opens questions regarding timing of the GB uplift and magnitude of the collapse events. As the major uplift is estimated to be Upper Miocene, the larger collapse cycles are expected to occur within the sequence bound by horizons H1 and H2. Our data corroborate this, but the size of MTD1 (and other lateral equivalents) suggests the occurrence of pre-Tortonian destructive events of similar magnitude to the ones of the currently considered major uplift stage. Thus, high magnitude collapse events could already be taking place since the onset of tectonic compression and mantellic exhumation in the Middle Miocene. The timing and location of the Miocene MTDs indicate that the locus of failure-triggering, uplift-related earthquakes alternated between the southern and northern sectors along the whole structure of the GB, separated by the structural saddle between the Ormonde and Gettysburg seamounts (Figs. 8 and 9). A Miocene earthquake trigger for regional mass-movements is further supported by the Chaotic Body on the Horseshoe Abyssal Plain (Supplementary Material 1) and associated olistostrome, both markers of the wider tectonism on the SWIM (Sallarès et al., 2013).

Markedly distinct flank collapse episodes are recorded by the Pliocene-Quaternary MTDs, which cluster on the northern sector of the GB (Fig. 9). These are smaller or thinner than Miocene ones (Supplementary Material 3), and their lower magnitude trigger events correlate with the post-Miocene tectonic quiescence on the margin (Terrinha et al., 2019; Tortella et al., 1997). However, MTD8 proves that larger collapses are prone to occur and constitute tsunami hazards in the region (Lo Iacono et al., 2012). The predominance of MTDs towards the north suggests that failure-triggering earthquakes tended to cluster within this sector (Fig. 9). These may take place along reactivated faults of the Mesozoic syn-rift detachment. The post-depositional deformation of Miocene-age MTDs shown in Figs. 3 and 6, namely MTD3, supports the premise of a continuum of deformation and fault reactivation predominantly to the north. Likewise, the less evident post-depositional deformation of the Late Miocene MTDs and the lack of very large (seismically resoluble) Pliocene-Quaternary MTDs on the southern sector suggests a relative stability of the latter (Figs. 3 and 5b). The distribution of the Pliocene-Quaternary MTDs further supports the clear structural compartmentalisation on the GB, with recent deformation events predominating where crustal basement rocks, higher fault densities and seismicity clustering are observed (Fig. 9). A full link between seismicity and mass-wasting on the GB is, however, not achievable with the available dataset. The majority of seismic events likely does not produce a slope failure, let alone large ones. Furthermore, lower magnitude slope failures may either create small-scale deposits well below the seismic resolution or leave no deposit at all. However, our goal was to depict broad collapse scenarios on the seamount and not tackle such still open questions on the fine relationships between seismicity and mass-failures.

5.2. Morphological rejuvenation of tectonic seamounts

On volcanic seamount lifecycles, the later-life phase is marked by destructive events as they drift away from volcanic centres (Fig. 10). This leaves a morphological record expressed as flank scars and surrounding MTDs as the seamount size decreases (Hunt

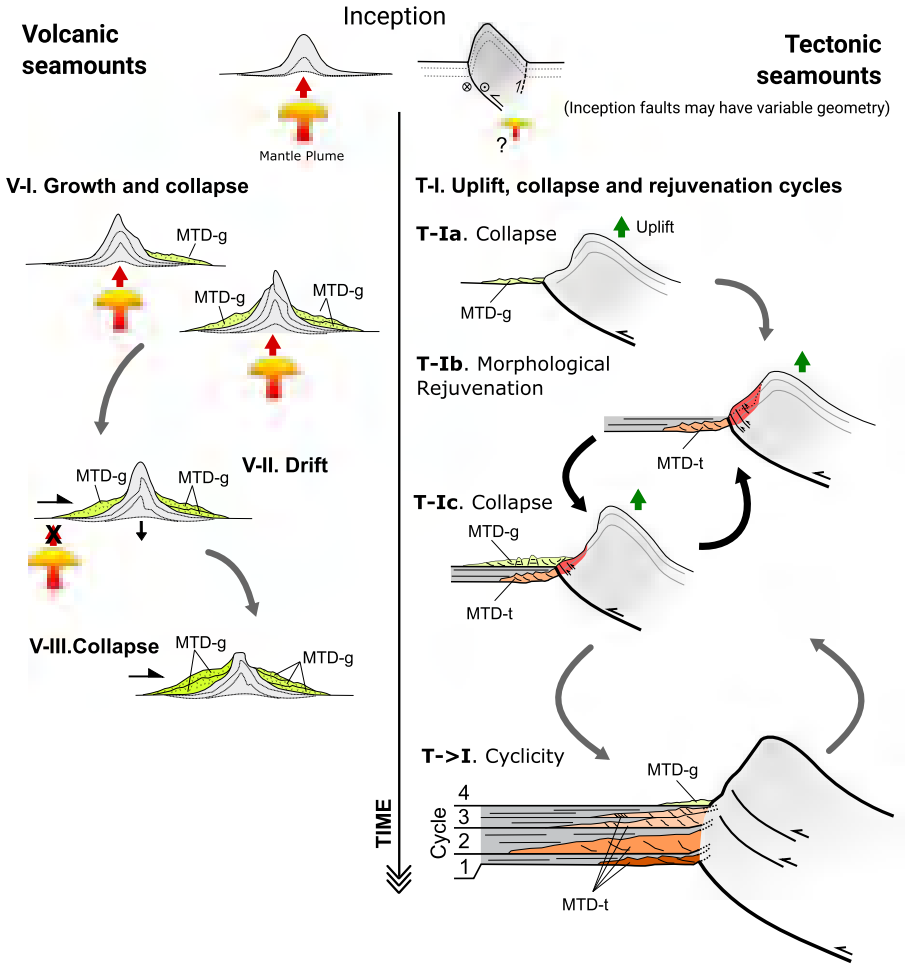

Fig. 10. Conceptual model of volcanic and tectonic seamount lifecycles. Volcanic seamount evolution is marked by constructive and destructive events while overlying the inception eruptive centre (**V-I**). As they drift away (**V-II**) subsidence and destructive events prevail, leading to cumulative degradation of the volcanic seamount (**V-III**). Tectonic seamount inception is controlled by thrust, normal and/or transform faults, often with volcanic inputs. Collapse episodes occur, likely associated to earthquakes during uplift episodes, with MTDs only showing gravity-driven deformation (MTD-g) (**T-Ia**). During quiescent tectonic periods, continuous thrust activity forms frontal deformation wedges with seafloor morphological expression, hindering the evidence of past high magnitude MTDs, now buried and tectonised (MTD-t) (**T-Ib**). Posterior collapse episodes deposit new MTDs, which can remove portions of the deformation wedge (**T-Ic**). These cycles will repeat at different magnitudes during the tectonic seamount evolution, leaving a record of variable magnitude and increasingly tectonised MTDs the deeper they are buried (**T-> I**).

and Jarvis, 2020; Mitchell, 2003). While these premises are valid for tectonic seamounts, we propose that these tend to have more complex lifecycles marked by destructive and morphologic rejuvenation events (Fig. 10). The latter potentially mask or remove evidence of past catastrophic collapses from the seamount's flank, limiting evolutionary interpretations if derived only from their morphology.

The MTDs on the TAP and present-day morphology of the GB are used to support our morphological rejuvenation hypothesis. The premise derives from continuous deformation at the thrust front. At subduction fronts on collisional margins, thrust wedges create bulging topography as the hanging-wall advances. On the GB the same principle will apply. A frontal wedge likely developed along the whole GB northern flank during the Miocene uplift and associated shortening, pre-dating or synchronous to the occurrence of the large Miocene MTDs identified along the whole extent of the seamount. However, no clear scars correlatable to the magnitude or source of the large Miocene MTDs are present on the GB flank. Even interpreted larger scars are ambiguous, especially when multiple MTDs occur in the same area (as, for instance, MTDs 1, 3 and 7, Fig. 9). Furthermore, large Miocene MTDs could have remobilised the paleo-wedge, in the same way that MTD8 obliterated deformation indicators by removing a fraction of the younger wedge (Fig. 6b). In contrast, the younger deformation wedge is preserved and has topographic expression on the modern seafloor. Its extent is coincident with a three-way branching of the GB frontal thrusts (Figs. 2, 8 and 9), and is marked by gradient decrease of 2–3° between the middle and lower depths of the GB flank (Supplementary Material 2). The gradients outside the wedge limits are, however, steeper to the south (Supplementary Material 2) where recent MTDs are barely present. The wedge extent, its coincidence with the thrust faults, and the distribution of Pliocene-Quaternary MTDs (Fig. 9) support the interpretation that morphology-shaping tectonic deformation episodes are prevalent towards the north, and limited on the south. However, we cannot rule out that the steeper southern flanks and limited wedge deformation are not due to different thrust fault dynamics. Despite the limited numbers of MTDs identified ($n = 8$), their morphometry, distribution and timing still validate the hypothesis. Thus, the assessment of rejuvenation can be based on qualitative (or semi-quantitative) assessments inferred from the geological features observable on available data. Furthermore, this opens the door for future open questions on quantitative model validation based on event recurrence and detailed age constrains if or when more thorough, multi-scale datasets are available from tectonic seamount study areas. The morphological rejuvenation events may therefore take place at seamount segments where tectonic activity is prevalent, hindering the indicators of past massive collapses. Further evidence for this is provided by

strata imbrications and thrusts observed within the deformation wedge (Figs. 5, 7 and 8). The flank proximal packages can effectively be considered as a localised tectonic mélange derived from the thrusting of the GB over the TAP, which reworked portions of the older MTDs. The gentle tilting of Miocene MTDs to the south (Fig. 5c), compared to their faulting, folding and higher tilt to the north (Fig. 5a), is yet another indicator for enhanced tectonism on the latter. Further to the role of the thrust faults, the top of the wedges likely includes gravitational deformation products associated with creep and low magnitude slumping that, in conjunction with ocean current reworking, further reshape and smooth the surface. The use of the GB as a model template can raise questions on its global validation given the likely variability of tectonic seamounts. The GB-based model would also need to be primarily tested on tectonic seamounts on compressive or transpressive stress regimes. The Ampere and Coral Patch tectonic seamounts located to the SW of the GB (Fig. 1) are tests candidates that share a similar evolution to the GB (Sartori et al., 1994). However, data coverage on this area is limited (Fig. 1) and seismic surveys are absent, mirroring the issues of data availability for seamount studies. Further questions still prevail, as we did not tackle the record of large MTDs derived from the GB SE flank (mostly because such deposits are absent there), but elsewhere there could be cases with large MTDs on both flanks of tectonic seamounts. Would there be rejuvenation on both flanks? The model would also need to be tested on tectonic seamounts on extensional regimes in order to assess if rejuvenation would occur, or if these would be ruled by morphological degradation. These are issues that future research may address.

To summarise, our conceptual model of morphological rejuvenation of thrust fronts during the lifecycle of tectonic seamounts starts with its inception and initial uplift (Fig. 10). Earthquake-triggered MTDs will occur associated to individual uplift stages and shortly after, degrading the flank morphology with marked scars and sediment evacuation (Fig. 10, T-Ia). Continuous compression develops a frontal wedge that hinders past scars, creates morphological relief, and deforms existing MTDs (Fig. 10, T-Ib). On the long term, there is no marked continuous loss of topography on the seamount's flank. New collapse events will take place during destructive episodes, degrading the rejuvenated morphology (Fig. 10, T-Ic). These cycles repeat over time (Fig. 10, T > I), dictated by the dynamics of the regional tectonics. The magnitude of the collapses is proportional to the magnitude and rate of the uplift or thrust advance. The locus of the inter-collapse tectonic events and morphological rejuvenation can take place along the whole structure or be restrained to tectonic compartments with enhanced activity (Fig. 9). From a geohazard perspective, our concept postulates that despite the limited morphological evidence on modern tectonic seamount flanks, catastrophic flank collapses may have occurred in the past. Thus, they may repeat in the future during the seamount's lifecycle and pose relevant geohazards.

6. Conclusions

Our results reveal (at least) two generations of MTDs deposited on the TAP sourced from the northwestern flank of the GB. During the Miocene uplift stage of the GB, large slope failures occurred along the structure length, associated with trigger events of likely seismic nature on the whole paleo-GB. Posterior Pliocene-Quaternary MTDs deposited during a stage of tectonic quiescence. These are smaller and predominantly occur on the northern sector of the GB's thrust flank, although a large blocky MTD is also present. The spatial clustering of Pliocene-Quaternary MTDs indicates that tectonic movements and associated seismicity focus towards the north in comparison to south. The morphometry and relative timing of the MTDs indicate that the magnitude of the collapse events is proportional to the magnitude of tectonic activity on the GB. Based on the analysis of destructive episodes and the modern morphology of the GB, we propose an evolutionary model where morphological rejuvenation driven by tectonic deformation at thrust fronts occurs multiple times on the lifecycle of tectonic seamounts. Such hinders the vestige of past catastrophic events on tectonic seamounts, only discernible if sub-surface data is available, thus limiting the understanding of the geohazard potential of these important submarine features.

CRediT authorship contribution statement

Davide Gamboa: Conceptualization, Formal analysis, Investigation, Writing – original draft, Writing – review & editing. **Rachid Omira:** Conceptualization, Funding acquisition, Project administration, Resources, Writing – review & editing. **Aldina Piedade:** Visualization. **Pedro Terrinha:** Data curation, Resources, Writing – review & editing. **Cristina Roque:** Writing – review & editing. **Nevio Zitellini:** Resources, Writing – review & editing.

Acknowledgements

This work is supported by the project MAGICLAND - MArine Geo-hazards InduCed by underwater LANDslides in the SW Iberian Margin (Ref: PTDC/CTA-GEO/30381/2017), funded by the Fundação para a Ciência e Tecnologia (FCT), Portugal. The authors wish also to acknowledge the financial support of FCT through project UIDB/50019/2020 – IDL. The Direcção Geral de Energia e Geologia (DGEG) is greatly acknowledged for the provision and permission to use part of the seismic data here presented. We thank the help of Dina Vales for the provision of earthquake data, João Duarte for the provision of regional tectonic information, and João Noiva for all the technical support provided. Halliburton is acknowledged for the provision of the DecisionSpace 10 seismic interpretation software bundle. We thank Dr James Hunt and an anonymous reviewer for their comments and insights towards the preparation of the final manuscript.

Declaration of competing interest

The authors declare that they have no known competing financial interests or personal relationships that could have appeared to influence the work reported in this paper.

Appendix A. Supplementary material

Supplementary material related to this article can be found online at https://doi.org/10.1016/j.epsl.2021.116772.

References

Alves, T.M., Gamboa, D., 2019. Mass-transport deposits as markers of local tectonism in extensional basins. In: Ogata, K., Festa, A., Pini, G.A. (Eds.), Submarine Landslides: Subaqueous Mass Transport Deposits from Outcrops to Seismic Profiles. In: AGU Geophysical Monograph Series, pp. 71–90.

Banda, E., Torne, M., Group, I.A.M., 1995. Iberian Atlantic Margins Group investigates deep structure of ocean margins. Eos, Trans. Am. Geophys. Union 76, 25–29.

Baptista, M.A., Miranda, P., Miranda, J.M., Victor, L.M., 1996. Rupture extent of the 1755 Lisbon earthquake inferred from numerical modeling of tsunami data. Phys. Chem. Earth 21, 65–70.

Bulhões, É.M., de Amorim, W.N., 2005. Princípio da SismoCamada Elementar e sua aplicação à Técnica Volume de Amplitudes (tecVA). In: 9th International Congress of the Brazilian Geophysical Society. European Association of Geoscientists & Engineers. pp. cp-160-00352.

Bull, S., Cartwright, J., Huuse, M., 2009. A review of kinematic indicators from mass-transport complexes using 3D seismic data. Mar. Pet. Geol. 26, 1132–1151.

Chopra, S., Marfurt, K.J., 2007. Seismic attributes for prospect identification and reservoir characterization. Society of Exploration Geophysicists and European Association of Geoscientists and Engineers.

Custódio, S., Dias, N.A., Carrilho, F., Góngora, E., Rio, I., Marreiros, C., Morais, I., Alves, P., Matias, L., 2015. Earthquakes in western Iberia: improving the understanding of lithospheric deformation in a slowly deforming region. Geophys. J. Int. 203, 127–145.

EMODnet Bathymetry Consortium, 2018. EMODnet Digital Bathymetry (DTM 2018). EMODnet Bathymetry Consortium.

Ferranti, L., Passaro, S., de Alteriis, G., 2014. Morphotectonics of the Gorringe Bank summit, eastern Atlantic Ocean, based on high-resolution multibeam bathymetry. Quat. Int. 332, 99–114.

Festa, A., Ogata, K., Pini, G.A., Dilek, Y., Alonso, J.L., 2016. Origin and significance of olistostromes in the evolution of orogenic belts: a global synthesis. Gondwana Res. 39, 180–203.

Fukao, Y., 1973. Thrust faulting at a lithospheric plate boundary the Portugal earthquake of 1969. Earth Planet. Sci. Lett. 18, 205–216.

Gamboa, D., Alves, T.M., 2016. Bi-modal deformation styles in confined mass-transport deposits: examples from a salt minibasin in SE Brazil. Mar. Geol. 379, 176–193.

Geldmacher, J., Hoernle, K., Klügel, A., Bogaard, P.v., Wombacher, F., Berning, B., 2006. Origin and geochemical evolution of the Madeira-Tore Rise (eastern North Atlantic). J. Geophys. Res., Solid Earth 111.

Girardeau, J., Cornen, G., Agrinier, P., Beslier, M.-O., Dubuisson, G., Le Gall, B., Monnier, C., Pinheiro, L., Ribeiro, A., Whitechurch, H., 1998. Preliminary results of nautile dives on the Gorringe Bank (West Portugal). C. R. Acad. Sci., Sér. IIA, Earth Planet. Sci. 4, 247–254.

Gràcia, E., Danobeitia, J., Vergés, J., Bartolomé, R., Córdoba, D., 2003. Crustal architecture and tectonic evolution of the Gulf of Cadiz (SW Iberian margin) at the convergence of the Eurasian and African plates. Tectonics 22 (4), 1033.

Gràcia, E., Vizcaino, A., Escutia, C., Asioli, A., Rodes, A., Pallas, R., Garcia-Orellana, J., Lebreiro, S., Goldfinger, C., 2010. Holocene earthquake record offshore Portugal (SW Iberia): testing turbidite paleoseismology in a slow-convergence margin. Quat. Sci. Rev. 29, 1156–1172.

Grevemeyer, I., Lange, D., Villinger, H., Custódio, S., Matias, L., 2017. Seismotectonics of the Horseshoe Abyssal Plain and Gorringe Bank, eastern Atlantic Ocean: constraints from ocean bottom seismometer data. J. Geophys. Res., Solid Earth 122, 63–78.

Gutscher, M.-A., Malod, J., Rehault, J.-P., Contrucci, I., Klingelhoefer, F., Mendes-Victor, L., Spakman, W., 2002. Evidence for active subduction beneath Gibraltar. Geology 30, 1071–1074.

Haq, B.U., Hardenbol, J., Vail, P.R., 1988. Mesozoic and Cenozoic chronostratigraphy and cycles of sea-level change. In: Wilgus, C.K., Hastings, B.S., Ross, C.A., Posamentier, H., Van Wagoner, J., Kendall, C.G.S.C. (Eds.), Sea-Level Changes - An Integrated Approach. In: SEPM Special Publication, vol. 42.

Hunt, J., Jarvis, I., 2020. The lifecycle of mid-ocean ridge seamounts and their prodigious flank collapses. Earth Planet. Sci. Lett. 530, 115867.

Jiménez-Munt, I., Fernandez, M., Vergés, J., Afonso, J.C., Garcia-Castellanos, D., Fullea, J., 2010. Lithospheric structure of the Gorringe Bank: insights into its origin and tectonic evolution. Tectonics 29, TC5019. https://doi.org/10.1029/2009TC002458.

Lo Iacono, C., Gràcia, E., Zaniboni, F., Pagnoni, G., Tinti, S., Bartolomé, R., Masson, D.G., Wynn, R.B., Lourenço, N., Pinto de Abreu, M., 2012. Large, deepwater slope failures: implications for landslide-generated tsunamis. Geology 40, 931–934.

Mauffret, A., Mougenot, D., Miles, P.R., Malod, J.A., 1989. Cenozoic deformation and Mesozoic abandoned spreading centre in the Tagus Abyssal Plain (west of Portugal): results of a multichannel seismic survey. Can. J. Earth Sci. 26 (6), 1101–1123.

Masson, D., Harbitz, C., Wynn, R., Pedersen, G., Løvholt, F., 2006. Submarine landslides: processes, triggers and hazard prediction. Philos. Trans. R. Soc., Math. Phys. Eng. Sci. 364, 2009–2039.

Mitchell, N.C., 2003. Susceptibility of mid-ocean ridge volcanic islands and seamounts to large-scale landsliding. J. Geophys. Res., Solid Earth 108.

Moscardelli, L., Wood, L., 2016. Morphometry of mass-transport deposits as a predictive tool. Geol. Soc. Am. Bull. 128, 47–80.

Mountjoy, J.J., Georgiopoulou, A., Chaytor, J., Clare, M.A., Gamboa, D., Moernaut, J., 2020. Subaqueous mass movements in the context of observations of contemporary slope failure. In: Georgiopoulou, A., Amy, L.A., Benetti, S., Chaytor, J.D., Clare, M.A., Gamboa, D., Haughton, P.D.W., Moernaut, J., Mountjoy, J.J. (Eds.), Subaqueous Mass Movements and their Consequences: Advances in Process Understanding, Monitoring and Hazard Assessments. Geological Society, London, Special Publications 500, pp. 1–12.

Neves, M., Terrinha, P., Afilhado, A., Moulin, M., Matias, L., Rosas, F., 2009. Response of a multi-domain continental margin to compression: study from seismic reflection–refraction and numerical modelling in the Tagus Abyssal Plain. Tectonophysics 468, 113–130.

Omira, R., Ramalho, I., Terrinha, P., Baptista, M.A., Batista, L., Zitellini, N., 2016. Deep-water seamounts, a potential source of tsunami generated by landslides? - The Hirondelle seamount, NE Atlantic. Mar. Geol. 379, 267–280.

Palmiotto, C., Corda, L., Bonatti, E., 2017. Oceanic tectonic islands. Terra Nova 29, 1–12.

Peirce, C., Barton, P., 1991. Crustal structure of the Madeira-Tore Rise, eastern North Atlantic—results of a DOBS wide-angle and normal incidence seismic experiment in the Josephine Seamount region. Geophys. J. Int. 106, 357–378.

Posamentier, H., Martinsen, O.J., 2011. The character and genesis of submarine mass-transport deposits: insights from outcrop and 3D seismic data. In: Shipp, C., Weimer, P., Posamentier, H. (Eds.), Mass-Transport Deposits in Deepwater Settings. In: SEPM Special Publication, vol. 96, pp. 7–38.

Purdy, G.M., 1975. The eastern end of the Azores-Gibraltar plate boundary. Geophys. J. Int. 43, 973–1000.

Ramos, A., Fernández, O., Terrinha, P., Muñoz, J.A., 2017. Neogene to recent contraction and basin inversion along the Nubia-Iberia boundary in SW Iberia. Tectonics 36, 257–286.

Rovere, M., Ranero, C.R., Sartori, R., Torelli, L., Zitellini, N., 2004. Seismic images and magnetic signature of the Late Jurassic to Early Cretaceous Africa-Eurasia plate boundary off SW Iberia. Geophys. J. Int. 158, 554–568.

Sallarès, V., Martínez-Loriente, S., Prada, M., Gràcia, E., Ranero, C., Gutscher, M.-A., Bartolome, R., Gailler, A., Dañobeitia, J.J., Zitellini, N., 2013. Seismic evidence of exhumed mantle rock basement at the Gorringe Bank and the adjacent Horseshoe and Tagus abyssal plains (SW Iberia). Earth Planet. Sci. Lett. 365, 120–131.

Sarma, K., Ramana, M., Subrahmanyam, V., Krishna, K., Ramprasad, T., Desa, M., 1998. Seamounts an additional tool to confirm the nature of the crust and to locate possible mineral resources for dredging. Mar. Georesour. Geotechnol. 16, 41–51.

Sartori, R., Torelli, L., Zitellini, N., Peis, D., Lodolo, E., 1994. Eastern segment of the Azores-Gibraltar line (central-eastern Atlantic): an oceanic plate boundary with diffuse compressional deformation. Geology 22, 555–558.

Schmidt, R., Schmincke, H.-U., 2000. Seamounts and island building. In: Sigurdsson, H., Houghton, B., Mc-Nutt, S., Rymer, H., Stix, J. (Eds.), Encyclopedia of Volcanoes. Academic Press, San Diego, California, pp. 383–402.

Siebert, L., 1984. Large volcanic debris avalanches: characteristics of source areas, deposits, and associated eruptions. J. Volcanol. Geotherm. Res. 22, 163–197.

Silva, S., Terrinha, P., Matias, L., Duarte, J.C., Roque, C., Ranero, C.R., Geissler, W.H., Zitellini, N., 2017. Micro-seismicity in the Gulf of Cadiz: is there a link between micro-seismicity, high magnitude earthquakes and active faults? Tectonophysics 717, 226–241.

Staudigel, H., Clague, D.A., 2010. The geological history of deep-sea volcanoes: biosphere, hydrosphere, and lithosphere interactions. Oceanography 23, 58–71.

Terrinha, P., Kullberg, J.C., Neres, M., Alves, T., Ramos, A., Ribeiro, C., Mata, J., Pinheiro, L., Afilhado, A., Matias, L., 2019. Rifting of the Southwest and West Iberia Continental Margins. In: Quesada, C., Oliveira, J.T., Vergés, J., Kullberg, J.C. (Eds.), The Geology of Iberia: A Geodynamic Approach. Volume 3: The Alpine Cycle. Springer International Publishing, Cham, pp. 251–283.

Tontini, F.C., de Ronde, C., Kinsey, J., Soule, A., Yoerger, D., Cocchi, L., 2013. Geophysical modeling of collapse-prone zones at Rumble III seamount, southern Pacific Ocean, New Zealand. Geochem. Geophys. Geosyst. 14, 4667–4680.

Tortella, D., Torne, M., Pérez-Estaún, A., 1997. Geodynamic evolution of the eastern segment of the Azores-Gibraltar zone: the Gorringe Bank and the Gulf of Cadiz region. Mar. Geophys. Res. 19, 211–230.

Vergés, J., Kullberg, J.C., Casas-Sainz, A., de Vicente, G., Duarte, L.V., Fernàndez, M., Gómez, J.J., Gómez-Pugnaire, M.T., Sánchez, A.J., López-Gómez, J., 2019. An introduction to the Alpine cycle in Iberia. In: Quesada, C., Oliveira, J. (Eds.), The Geology of Iberia: A Geodynamic Approach. In: Regional Geology Reviews. Springer, Cham, pp. 1–14.

Zitellini, N., Gràcia, E., Matias, L., Terrinha, P., Abreu, M., DeAlteriis, G., Henriet, J., Dañobeitia, J., Masson, D., Mulder, T., 2009. The quest for the Africa–Eurasia plate boundary west of the Strait of Gibraltar. Earth Planet. Sci. Lett. 280, 13–50.

Zitellini, N., Mendes, L., Cordoba, D., Danobeitia, J., Nicolich, R., Pellis, G., Ribeiro, A., Sartori, R., Torelli, L., Bartolomé, R., 2001. Source of 1755 Lisbon earthquake and tsunami investigated. Eos, Trans. Am. Geophys. Union 82, 285–291.